

## On the features of breaking a microjet of dilute polymer solution into main and satellite microdroplets under external vibration perturbation

© N.A. Khomutov, A.E. Semyonova, M.V. Belonogov, Antonio Di Martino, E.A. Khan, M.V. Piskunov

Tomsk Polytechnic University, Tomsk, Russia  
e-mail: streetstoryteller@gmail.com

Received August 3, 2022

Revised October 14, 2022

Accepted October 19, 2022

An experimental study of the morphology of the laminar microjet flow of diluted aqueous solutions of sodium alginate without and with the addition of hydroxyethyl cellulose after a nozzle subject to external vibration stimulation by the action of the reverse piezoelectric effect was carried out. We studied the influence of the polymer concentration in the solution (0.5–5 mg/ml), the flow rate of the liquid (4–26 ml/min), and the frequency of the current of external perturbation (0–1.2 kHz) on the capillary crushing of the microjet with a diameter of about 210  $\mu\text{m}$  in the range of Ohnesorge numbers from 0.046 to 1.88 and Reynolds numbers 0.7 to 470. The modes of microjet flow and crushing on microdroplets with indication of boundaries of transitions between them are selected, and a general map of modes is built. Taking into account the polymer concentration in the solution, the dependence of the microjet fracture length on its velocity is shown. The conditions of monodisperse microjet destruction with equidistant arrangement of the main microdroplets in the flow are determined, which are related to an optimal balance between the molecular mass of the polymer in the solution, the intensity of external disturbance and the time of stress relaxation in polymer viscoelastic microjets. The role of formation of structures such as „beads-on-filament“ in capillary destruction of microjet with identification of cases of absence of occurrence of „satellite“ microdroplets from liquid threads between the main microdroplets has been studied. The results are applied to technologies based on in-air microfluidics (bioengineering and additive technologies), dealing with heterogeneous fluids with viscoelastic properties.

**Keywords:** Plateau–Rayleigh instability, reverse piezoelectric effect, monodisperse breakup, relaxation time, microjet flow.

DOI: 10.21883/TP.2023.01.55437.198-22

### Introduction

The controlled breakup of a laminar jet into microdrops is a key step in existing and advanced processes such as jet printing [1], encapsulation [2,3], additive manufacturing [4], microfluidics [5], especially in-air microfluidics [3,6]. For many of these processes the formation of satellite drops, i.e. considerably less in size liquid fragments, that are formed between main drops of the broken jet, which is ubiquitous in the breakup of low-viscosity fluids [7], is detrimental to these applications and must be controlled. This phenomenon is especially actual, because production cycles and research laboratories actively engage liquids with complex internal structure and composition of components, that, as it was shown by experiments with drops and jets [5,7–11], have significant differences and distinctive morphological features in the liquid dynamics as compared with homogeneous compounds.

The breakup of homogeneous Newtonian liquid jets into droplets is rather well studied by now [12,13]. It is important to note the classical studies where attempts have been made to explain the laws of satellite drops formation [14,15] and even to control sizes of the main and satellite drops [15]. It is found that changes in the

perturbation wavelength, the perturbation magnitude, and the Weber number ( $We$ ) are considered as the main factors that influence the formation of drops and their sizes.

The situation with investigations of heterogeneous liquid jets is not so unambiguous. On one hand, the extensive development of jet printing technologies that use inks with complex compositions of components from 1970-es [12,14] promoted the development of currently in-demand technologies in the field of biological engineering and additive manufacturing [3,16]. These technologies are often based on liquids with unique compositions of components and structures, for example, polymer solutions [3], and liquids that demonstrate viscoelastic properties [5,7]. On the other hand, for all these applications, as it is noted in the above-referred works, the presence of bimodal size distribution of drops, i.e. the formation of satellite drops along with the main drops, remains a problem so far.

There are different approaches to the organization of microjet flow that make for the achievement of conditions for the ordering of elements within the formed microdrop flow in terms of its morphology (modes, where microdrops are „aligned“) and drop sizes. Among the main of them is physical cutting of the jet flow into monodisperse droplets using an additional device based on cut wire [17], which

Component composition of aqueous solutions of polymers and their properties

№	Denomination of composition	Polymer concentration in the solution ( $\varphi$ ), mg/ml	Mass ratio ALG:HEC	$\mu$ , mPa·s	$\sigma$ , mN/m	$\rho$ , kg/m <sup>3</sup>
1	0.5 mg/ml ALG + HEC	0.5	5:1	4.68	53.0 ± 0.2	955
2	2.5 mg/ml ALG + HEC	2.5	5:1	18.93	56.4 ± 0.1	1003
3	5 mg/ml ALG	5	–	205	58.6 ± 0.2	1021

main disadvantage is the loss of liquid resulted from the flow cutting. Other approaches are the electrostatic and vibration external impact on the nozzle tip [3,18,19], which fine tuning for a specific liquid allows achieving the desired results in terms of monodisperse distribution of drop sizes. The quoted studies show, that the controlled breakup of microjets into microdrops due to an external impact (electrostatic field, inverse piezoelectric effect) has a number of disadvantages, including, first of all, the fine tuning of the system for the certain liquid composition, and, in addition, the passivity of viscous liquids (for example, polymer solutions) in response to such impact. Thus, experiments with promising unique (heterogeneous, Newtonian) compositions used or having a potential for use in a specific practical application are currently in demand and actual for the purpose of forming a general theoretical basis. In this work, we are focused on the experimental studying of the detailed morphology of laminar microjet flow of sodium alginate aqueous solutions with and without addition of hydroxyethyl cellulose (as a solution thickener) downstream of the nozzle, which is exposed to an external vibration impact due to implementation of the inverse piezoelectric effect, with distinguishing characteristic modes. The studying of flow morphology will include features of microjet and microdrop flows taking into account poly- and mono- dispersity of the drop size distribution. This task has an applied significance for the technologies based on the in-air microfluidics, which are currently the subject of the most advanced research activities in the field of „drop–jet“ type interactions [3,6,18,20–22] with „complex“ liquids.

This experimental investigation is motivated by the detailed study of the approach of controlled breakup of biocompatible polymers aqueous solutions under the inverse piezoelectric effect proposed in [3]. According to the authors, the investigation detailing is needed to identify behavioral patterns (systems of arrangement within flow) of main and satellite microdrops and conditions of transitions between them, as well as the conditions that prevent formation of the latter. This reflects the scientific novelty and practical significance of the works with regard to the technologies of additive manufacturing of three-dimensional modular structures using methods of in-air microfluidics [3,6,18].

## 1. Materials

To investigate the process of microjet breakup, we used aqueous solutions of sodium alginate without and with addition of hydroxyethyl cellulose (with a mass ratio of 5:1, respectively) as a thickener and as a viscosity controller in general. Sodium alginate (ALG) — a linear polysaccharide — is widely used in many biological engineering applications, for example, in three-dimensional bioprinting [3]. Hydroxyethyl cellulose (HEC) — an amino acid of vegetable origin — is used in hydrogels [23] to achieve slower release of water as compared to the solutions based on sodium alginate only, has an effect on the absorption of water and biodegradation of the final material. Both polymers are water-soluble, bio-compatible, and capable of biodegradation. The table lists solutions used and specifies their properties: dynamic viscosity ( $\mu$ ), surface tension coefficient at the „liquid–air“ interface ( $\sigma$ ), and density ( $\rho$ ).

Viscosity of investigated liquids was determined with a Brookfield DV3T LV rotational viscometer (with a accuracy of  $\pm 1\%$ , a measuring range of  $1-6 \cdot 10^6$  mPa · s). The table presents mean values of viscosity measured at shear rates of 10 and 50 1/s. The surface tension coefficient at the „air–liquid“ interface was determined by the method of du Nouy (semistatic method to determine the surface tension) using a Kruss K20 tensiometer (with an accuracy of  $\pm 1\%$ , a measurement range of 1–999 mN/m). Density of liquids was determined by the picnometer method. To minimize the random error, at least three series of measurements were performed for each sample under identical conditions.

Molecular masses ( $M_w$ ) of polymers used in this study were  $215 \pm 35$  kDa for the salt of alginic acid (sodium alginate) and 90 kDa for HEC. The value of  $M_w$  for HEC is provided by the manufacturer (Sigma–Aldrich). Values of  $M_w$  for sodium alginate are evaluated on the basis of rotational viscometry data (see the table) and the data yielded from the Mark–Kuhn–Houwink equation  $[\mu] = KM_w^\alpha$  for the relation between the characteristic viscosity of polymer in solution and its molecular mass, where  $[\mu]$  — characteristic viscosity, [dl/g],  $K$  and  $\alpha$  — constants for a specific polymer–solvent system.

Relaxation times of stresses in the polymer solutions in question are determined from relationship (1) for the calculation of filament diameter  $d_f$  at a moment of time  $t$ ,

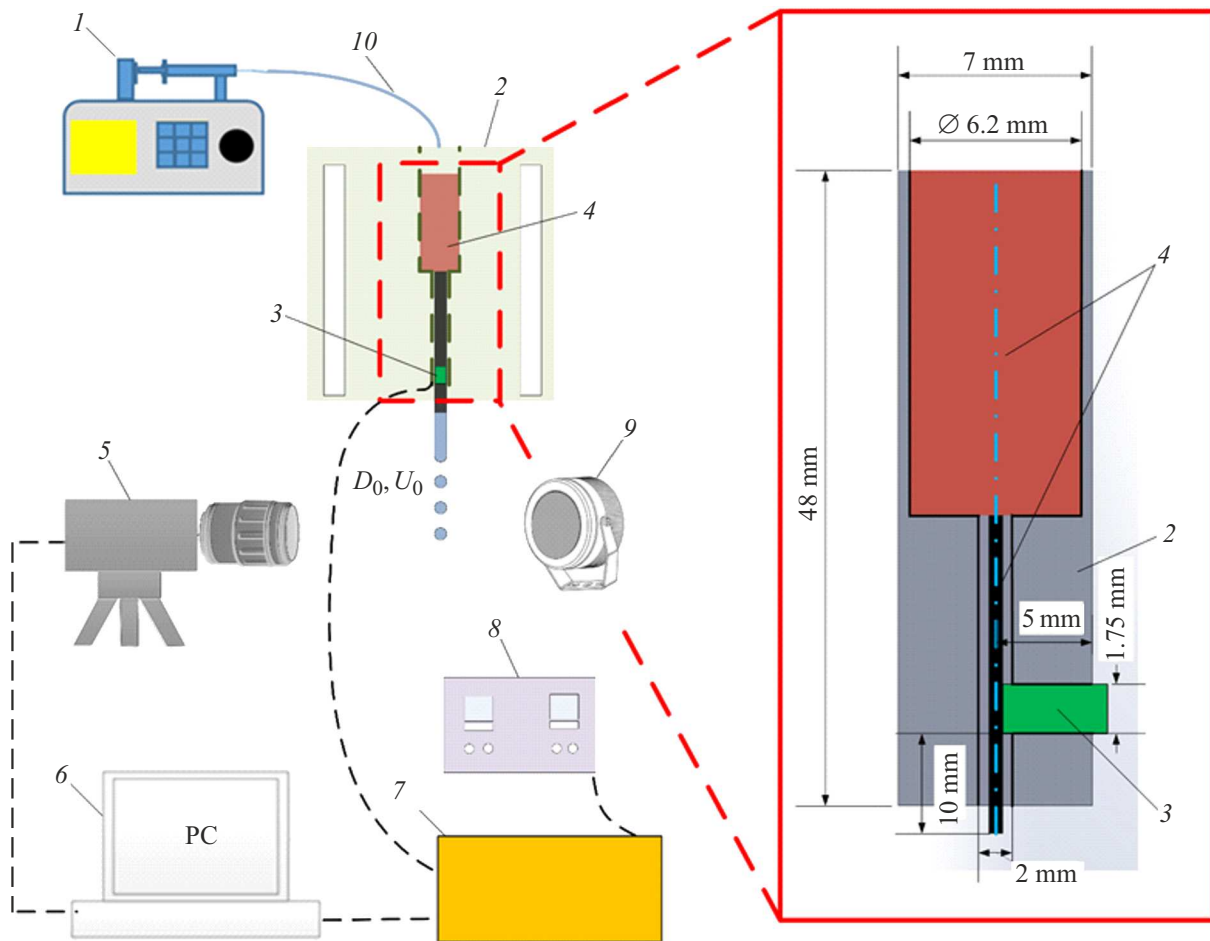


**Figure 1.** Experimental stand diagram (a); schematic sketch of the frame to fix the needle, side view (b): 1 — syringe pump, 2 — frame to fix the needle, 3 — piezoactuator, 4 — nozzle-hollow needle, 5 — high-speed video camera, 6 — PC, 7 — system to apply and amplify signal, 8 — power supply unit, 9 — lighting system, 10 — hose for polymer pumping.

which is an asymptotic solution to the equation for thin Maxwell fluid filament with the assumption of uniaxial extension of the cylinder connecting two spheres [24]. Microdrops are separated from the microjet of polymer liquid in the conditions of preliminary formed thin liquid filaments between future microdrops [7]. Diameters of these filaments  $d_f$  are measured in this work:

$$d_f = d_{f0} \exp\left(-\frac{t}{3\tau}\right), \quad (1)$$

where  $\tau$  — liquid relaxation time, [ms],  $d_{f0}$  — initial filament diameter, [m].

Time  $t$  was calculated as  $t = (d_{f0} - d_f) / U_j$ , where  $U_j$  — microjet velocity, [m/s], determined as a ratio of actual liquid flowrate ( $\text{m}^3/\text{s}$ ) to the cross-section area of microjet flow ( $\text{m}^2$ ).

## 2. Experimental stand

Fig. 1 shows the experimental setup intended to implement controlled breakup of a polymer liquid microjet into

monodisperse microdrops under the inverse piezoelectric effect.

The polymer was supplied by a SPLab02 syringe pump with the possibility to install syringes with Luer Lock type connection. This pump is designed to pump liquids with ultra-low flowrate (0.831 nl/min–152.9 ml/min) and high dosing accuracy ( $\pm 0.5\%$ ). A calibration curve is plotted showing the difference between actual (measured) flowrates of polymers solutions in question and values set on the pump (Fig. 2). The actual flowrate is measured with the use of volumetric glassware by determining the volume of liquid pumped during 1 min. In all calculations and in figures the actual liquid flowrate is used.

The liquid was supplied by a blunt tip syringe needle (with a metal part length of 4 cm, an inner diameter of 0.21 mm, and outer diameter of 0.4 mm). To fix the needle, a frame with required process holes (Fig. 1, a) was developed and printed out on a photopolymer 3D-printer. The plastic part of the needle was inserted into the grooves of the frame to be securely fixed, and metal part of the needle was placed in a special channel with a cross-section

of  $2 \times 2$  mm (Fig. 1, *a*). At a distance of 10 mm from the nozzle tip a square hole with a square side of 1.75 mm was made in the frame normally to the channel for the metal part to install a piezoactuator (Fig. 1, *b*).

The water-polymer solution flow was broken up using a multilayered piezoelectric actuator with dimensions of  $1.75 \times 1.75 \times 5$  mm (maximum working part travel is  $0\text{--}3.8\ \mu\text{m}$ , working stress range is  $U = 0\text{--}100$  V). To supply a stimulus signal to the piezoactuator and amplify it, a system was used consisting of an ADC module, a voltage amplifier, and a buffer voltage amplifier.

The external L-Card E14-140M ADC module connected to the PC via USB-port generated the stimulus signal. The working actuator knocked the needle surface in response to the stimulus signal. To set the signal, a program was written in the Labview software (National Instruments). This program allows generating of any signal profile, as well as setting the AC frequency ( $f = 0\text{--}2$  kHz), which is numerically equal to the number of piezoactuator oscillations. In this study the signal profile was represented by meander — a bipolar square signal. Current frequency  $f$  in this study varied from 200 to 1200 Hz.

To amplify the signal from the ADC module (5 V), a LM 4766t microchip (Texas Instruments) with operational amplifier was used. The implemented circuit of bridge amplifier allows supplying a voltage of  $\pm 30$  V to the piezoactuator. As a result, the maximum peak-to-peak voltage was as high as 60 V, which actually characterizes the piezoactuator compression at supply of +30 V and its expansion at  $-30$  V. The amplifier was powered by a QJ3005G III power supply unit (with an output voltage of  $0\text{--}30$  V in each adjustable channel, a setting accuracy of 0.1 V, an output current of  $0\text{--}5$  A in each adjustable channel, a setting accuracy of 0.01 A).

To prevent short circuiting, a buffer amplifier circuit was assembled in the ADC module in tended to match the output resistance of the signal source to the input resistance of the load. The system of buffer amplifier included L7812CV,

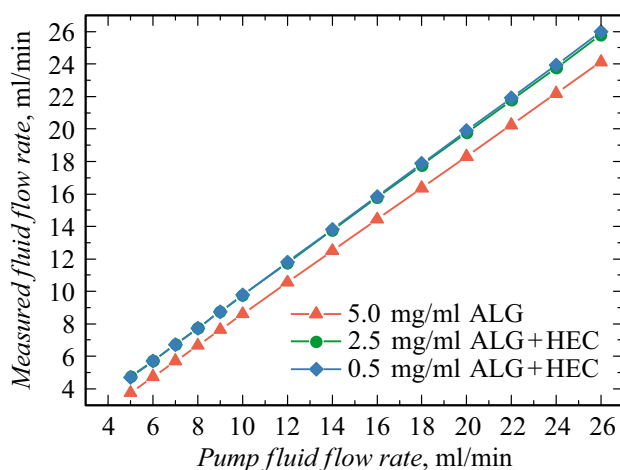


**Figure 2.** Calibration curve for the set and actual flowrates of polymer solutions.

L7912CV voltage stabilizers (ST Microelectronics) intended to keep the output voltage in a narrow range at significant changes in the input voltage and output current of the load, as well as a TL072 microchip (Texas Instruments).

The process of liquid jet breakup was video-recorded from the side at an angle of  $90^\circ$  in relation to the jet axis, using a Phantom Miro M310 high-speed video camera (with a recording rate of 10000 fps, a resolution of  $256 \times 800$  pixels). The backlighting system to support the high-speed „shadow“ video-recording included a GSVITEC MultiLED G8 power supply unit and two GSVITEC MultiLED QT spot lights with diffusers for light scattering.

### 3. Results and discussion

In all performed experiments the flow was broken up by two methods. The first method is a natural breakup of the polymer flow without the use of piezoactuator, i. e. a breakup resulted from the natural Rayleigh–Plateau instability. The second method assumes the use of a piezoactuator at a voltage of  $\pm 30$  V and  $f = 200\text{--}1200$  Hz. An external impact on the nozzle in the form of vibration resulted from the implementation of the inverse piezoelectric effect allows achievement of a controlled microjet breakup, where separation of monodisperse drops of the same size takes place, with the drops flowing within the controlled system of microdrop arrangement in the flow. In the following, we have investigated how the unsteady behavior of the microjet (in terms of morphology) depends on the polymer concentration (section 3.1.), solution flowrate (section 3.2.), and current frequency of the external impact (section 3.3.), with taking which into account microdrops can be ordered in the flow under the effect of vibration perturbation.

#### 3.1. Influence of polymer concentration in the solution on the capillary breakup of the microjet

To study the influence of polymer concentration in the solution (see the table) on the controlled microjet breakup under the effect of external vibration impact, experiments were performed at a constant liquid flowrate of 5 ml/min and  $f = 1000$  Hz.

In the course of experiments for all investigated liquids a controlled microjet breakup under piezoelectric effect was found starting from a perturbation current frequency of 1000 Hz. The separation of main drops from the microjet takes place in the conditions of formation of a thin liquid filament (a jumper or a little bridge; these structures are also known as „beads-on-string“ [7,25–27]) (Fig. 3), that becomes thin quickly and destabilizes into separate satellite microdrops with a size from a few micrometers to tens of micrometers. For the 5 mg/ml ALG solution, the length of microjet breakup is decreased by 20% as compared with the case of natural Rayleigh–Plateau instability (Fig. 4). The

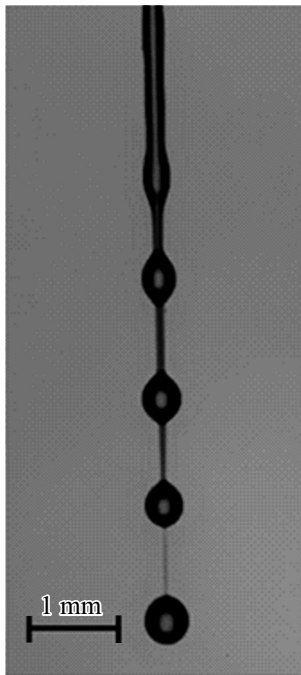


**Figure 3.** Formation of liquid filaments between microdrops of the 5 mg/ml ALG polymer solution at a liquid flowrate of 5 ml/min ( $U_j = 0.55$  m/s) and  $f = 1000$  Hz.

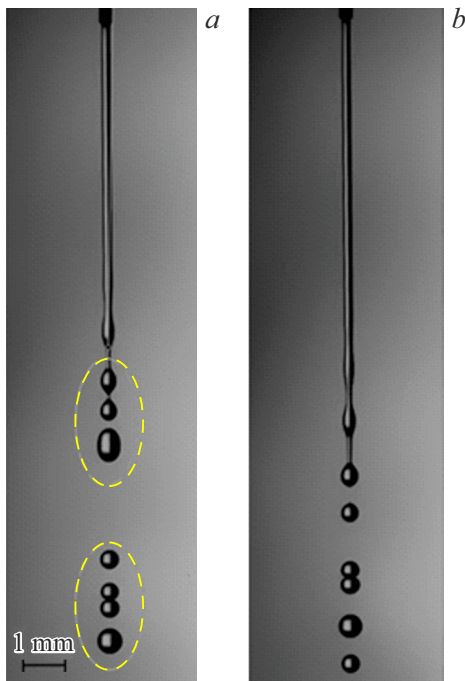


**Figure 4.** Visualization of the microjet breakup process for the 5 mg/ml ALG polymer solution at a liquid flowrate of 5 ml/min ( $U_j = 0.55$  m/s) and  $f = 1000$  Hz: *a* — controlled Rayleigh–Plateau instability (the „by groups“ mode); *b* — natural microjet instability without external impact.

feature consists in the microjet breakup by groups of 2–4 main drops each (Fig. 4, *a*).

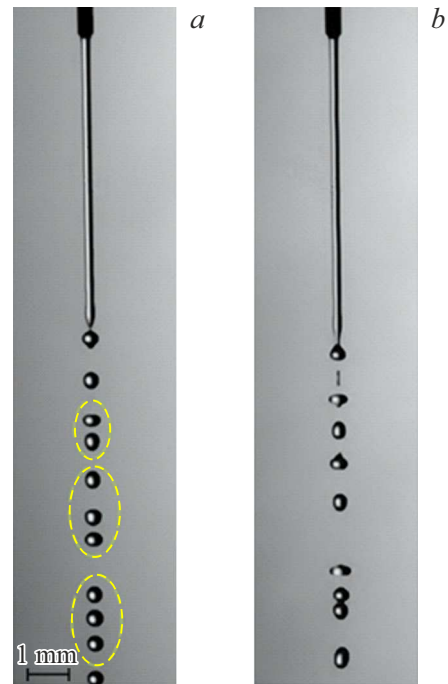


**Figure 5.** Visualization of the microjet breakup process for the 2.5 mg/ml ALG + HEC polymer solution at a liquid flowrate of 5 ml/min ( $U_j = 0.56$  m/s) and  $f = 1000$  Hz: *a* — controlled Rayleigh–Plateau instability (the „by groups“ mode); *b* — natural microjet instability without external impact.

As a rule, this is followed by a quick coalescence of the satellite drops formed in this way with the main drops moving upstream. It is found that the formation of liquid bridges slows down and perturbs the microjet breakup into monodisperse microdrops (main drops). With further movement of the flow, the filament becomes destabilized and the main microdrops move at a close distance to each other in the „by groups“ mode. For the purpose of comparison, Fig. 4, *b* shows unsteady behavior of a liquid flow without external impact.

For the 2.5 mg/ml ALG + HEC solution under an external impact, the length of microjet breakup is decreased by 5%, and the effect of vibration on the capillary microjet breakup also consists in the separation of main microdrops by groups of 2–4 drops each (Fig. 5, *a*), in contrast to the unordered formation of microdrops in the case of natural microjet instability (Fig. 5, *b*). However, in contrast to the 5 mg/ml ALG solution, in this case no liquid jumpers are observed between microdrops within a group (Fig. 5, *a*). This effect is explained by the setting for the 2.5 mg/ml ALG + HEC solution of a suitable optimum balance between the molecular mass of polymers in the solution ( $215 \pm 35$  kDa for sodium alginate and 90 kDa for HEC) and concentration of the substances (see the table), intensity of the external perturbation (current frequency of  $f = 1000$  Hz), and time of stress relaxation ( $\tau = 0.064$  ms) in polymer viscoelastic microjets [7]. In the case of the 5 mg/ml ALG solution

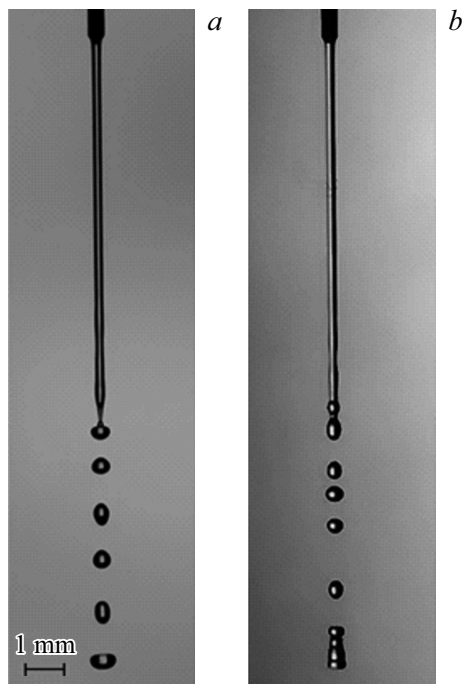


**Figure 6.** Visualization of the process of microjet breakup for the 0.5 mg/ml ALG + HEC polymer solution at a liquid flowrate of 5 ml/min ( $U_j = 0.55$  m/s) and  $f = 1000$  Hz: *a* — monodisperse capillary breakup of a microjet with equidistant main drops under the effect of forced perturbation; *b* — natural microjet instability without external impact.

(higher concentration of the polymer) no HEC is used and the relaxation time is higher ( $\tau = 0.083$  ms). The presence of liquid filaments in such studies is an indirect indication of the presence of viscoelastic properties (even their weak manifestation) of the investigated polymer material [4,7].

With the capillary breakup of a microjet of the 0.5 mg/ml ALG + HEC solution, the main microdrops become nearly equidistant from each other (Fig. 6, *a*) as compared to the case of the natural microjet instability (Fig. 6, *b*). It means that in contrast to two other investigated compositions (Fig. 4, *a*, 5, *a*), no groups of 2–4 drops are formed in this case, but a monodisperse breakup takes place with a certain frequency correlated with the intensity of the external vibration perturbation [7] caused by the inverse piezoelectric effect (i. e. first of all due to the current portion, which is supplied in a controllable manner). However, the shape of main microdrops is not spherical, which is most likely explained by a relatively low surface tension coefficient (see the table), i. e. low ratio of the surface energy to the area of free surface of the liquid, which is insufficient to compensate for the longitudinal deformations of the microjet caused by the forced perturbation (Fig. 6, *a*). The perturbation wavelength, in turn, defines the period of microjet oscillation at a longitudinal deformation [4,7].

Thus, an increase in polymer concentration in the solution results in the formation of groups of microdrops under

the capillary microjet breakup (2.5 mg/ml ALG + HEC and 5 mg/ml ALG solutions) and emergence of „beads-on-string“ type structures, which destabilize the microjet breakup process (the 5 mg/ml ALG solution). As it was noted earlier, due to the increase in polymer concentration and stress relaxation time a deviation takes place from the optimum balance [7], that defines the monodisperse microjet breakup in terms of both the size of main microdrops and the ordering of their movement (in the absence of satellite drops) with equal distance of the drops from each other. The obtained results correlate qualitatively with the conclusions made in [7,28].

### 3.2. Influence of liquid flowrate on the capillary microjet breakup

To evaluate the influence of liquid flowrate variation on the unsteady microjet behavior, experiments were performed at liquid flowrates of 4–26 ml/min with a set current frequency ( $f = 1000$  Hz) of the external perturbation for three investigated water-polymer solutions. Three modes of microjet flow observed at different liquid flowrates are distinguished. Fig. 7 shows typical frames for these modes for the example of 2.5 mg/ml ALG + HEC solution.

At low liquid flowrates (5–8 ml/min) the laminar flow of microjet has almost linear profile with hardly distinguishable perturbation amplitude and wavelength, i. e. the microjet under a perturbation impact has minimum curvature in relation to the flow axis (Fig. 7, *a*). With the liquid flowrate increasing up to 9–10 ml/min, a progression of

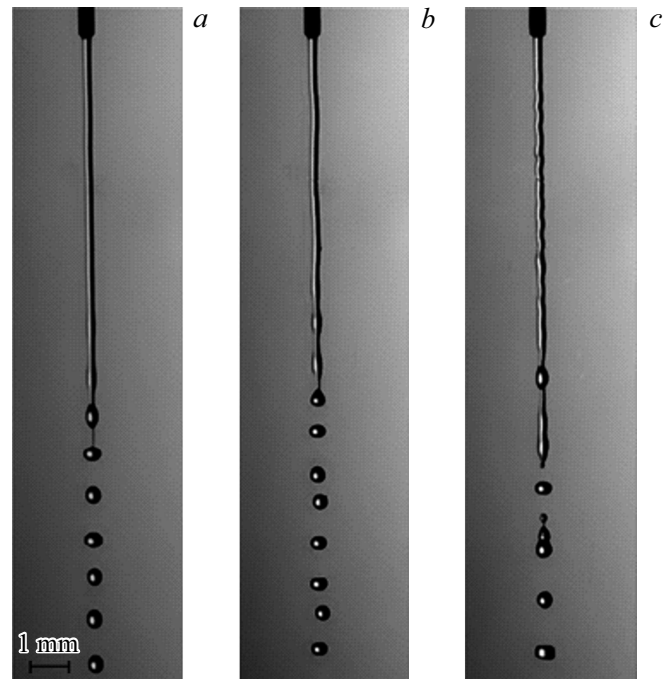


**Figure 7.** Visualization of the process of microjet breakup for the 2.5 mg/ml ALG + HEC polymer solution at an external vibration perturbation current frequency of  $f = 1000$  Hz and the following liquid flowrates: *a* — 5–8; *b* — 9–11; *c* — 12–26 ml/min.

microjet curvature is observed. It is reflected in a form of wavy deformation of the microjet profile in relation to the flow axis with a relative increase in perturbation amplitude and wavelength (Fig. 7, *b*). With further increasing liquid flowrate up to 12–26 ml/min, the perturbation amplitude and wavelength decrease significantly, while the microjet profile becomes saw-toothed (Fig. 7, *c*) with noticeably reconfiguring period of the oscillation.

Microjet behavior under the action of forced perturbation has a strong effect on the character of its breakup into main microdrops. The investigation of behavioral patterns (systems of arrangement in the flow) of main microdrops in conditions of liquid flow variation has shown that at 5–9 ml/min for the 0.5 mg/ml ALG + HEC solution a capillary breakup into disperse microdrops takes place, where the microdrops move equally distant from each other at least over a distance of 15–20 diameters of main microdrops from the point of microjet breakup (Fig. 6, *a* and 8, *a*). At the same time, for 2.5 mg/ml ALG + HEC and 5 mg/ml ALG solutions, at a liquid flowrate of 4–5 ml/min the mode of breakup „by groups“ of 2–4 main microdrops is noted, which is replaced by the monodisperse breakup even at a flowrate of 5–6 ml/min, depending on the liquid. For the 2.5 mg/ml ALG + HEC solution, the monodisperse breakup into microdrops was observed at a flowrate of 6–8 ml/min, and for the 5 mg/ml ALG solution it was observed even at 5–6 ml/min. At the same time, when liquid flowrates were 5–8 ml/min, mean (arithmetic) diameter of formed microdrops ( $d$ ) appeared to be the largest ( $d \approx 0.23$  mm) as compared with higher liquid flowrates. With increasing flowrates of liquids under test the breakup into microdrops has a monodisperse, irregular, but forecastable pattern. This is manifested in an offset of the microdrop flow path from the vertical axis, which is correlated with the positive and negative curvature of the microjet profile under a perturbation (Fig. 7, *b*), as well as in the possibility to forecast the arrangement of main microdrops in the flow (by groups of 2–4 microdrops) (Fig. 8, *a*). When the liquid flowrate was 10–24 ml/min for the 5 mg/ml ALG solution and 18–26 ml/min for two other liquids, the microdrop path was mainly coincided with the flow axis (Fig. 9), however in this case the external perturbation has completely disturbed the mechanism of microdrop separation (the Rayleigh–Plateau instability). At the same time, the condition of breakup polydispersion with significantly non-homogeneous space between the flowing microdrops has become relatively stronger (Fig. 7, *c*).

To summarize the morphological observations of laminar flow behavior of water-polymer solutions before and after breakup into microdrops, Fig. 8, *a* shows a chart of modes of microjet flow (see regions of different color) and breakup into microdrops (see shaded regions with different geometric symbols), demonstrating their boundaries in terms of liquid flowrates and polymer concentrations in solutions. The chart is plotted in a range of liquid flowrates of 4–26 ml/min and at a set external perturbation current frequency of ( $f = 1000$  Hz).

As a result of the analysis of microjet flow modes (Fig. 8, *a*), it was found that with an increase in the polymer concentration in the solution linearly profiled microjets (without deformation from an external perturbation) are observed in a wider range of liquid flowrates. The obtained result may be related to the amplifying influence of the liquid viscosity, when polymer concentration in the solution increases, as well as to a decrease in stress relaxation time in polymer materials. For the 5 mg/ml ALG solution, a microjet with a linear profile is observed at liquid flowrates of 4–8 ml/min. At the same time, for the 0.5 mg/ml ALG + HEC solution microjets with this type of profile are only observed at liquid flowrates of 5–6 ml/min. Critical values of stress relaxation times (for the polymer system return to the equilibrium state) determining the transition to another mode of microjet flow will be lower, the higher is fluid flowrate. In particular, for the 0.5 mg/ml ALG + HEC solution the critical value of  $\tau$  is 0.061 ms at a liquid flowrate of 6 ml/min, while for the 5 mg/ml ALG and 2.5 mg/ml ALG + HEC solutions critical values of  $\tau$  are approximately the same and equal to  $0.050 \pm 0.003$  ms at a liquid flowrate of 9 ml/min. Fig. 8, *a* also shows other modes of microjet flow (microjet with wavy profile, microjet with sawtooth profile) and the transition between them, which is connected in a similar way to the liquid flowrate and polymer concentration in the solution. Also, to summarize theoretically the morphological observations, a chart of microjet flow modes is built up using dimensionless similarity criteria (Fig. 8, *b*) — Ohnesorge numbers,  $Oh = \frac{\mu}{\sqrt{\sigma \rho D}}$ , and Reynolds numbers,  $Re = \frac{\rho U_j D}{\mu}$ , where  $D$  — diameter of the microjet, [m]. It can be seen, that, in general, with increase in viscous forces the formation region of microjets with linear profile is extended significantly. At the same time, in particular (for each liquid individually), growth of the  $Re$  number results in the above-described successive change of microjet modes. Transition between modes can be qualitatively described by a power function. Physical parameters of microjet, including those under analysis, are shown in Fig. 9 for clarity.

Meanwhile, the analysis of modes of microjet breakup into microdrops for the 0.5 mg/ml ALG solution has shown that monodisperse breakup is inherent for a rather wide range of liquid flowrates — 5–9 ml/min. It means that there are conditions of the controlled monodisperse breakup into microdrops, where the microjet profile before the capillary breakup can be both linear and wavy. This result confirms significance of the the forced vibration excitation intensity, which is responsible for the amplitude and wavelength of the microjet perturbation that, in turn, are dependent on the liquid flowrate to a significant extent. However, the intensity is strongly connected to the nature of the liquid itself (molecular mass of the polymer, its concentration in the solution, and stress relaxation if the material has even weak viscoelastic properties) [7]. An increase in polymer concentration in the solution makes narrower the range of liquid flowrates typical for the mode of monodisperse breakup into

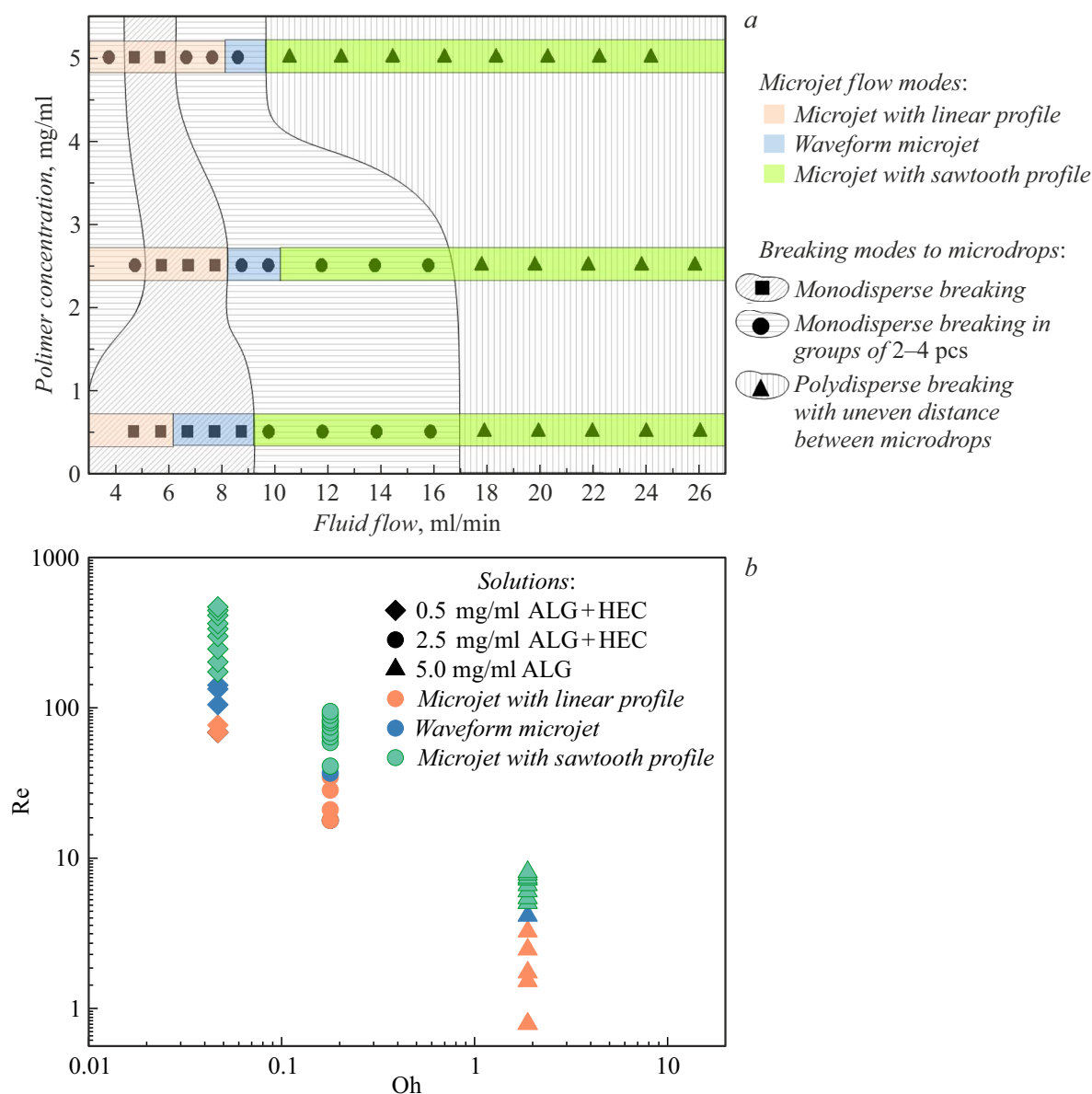


**Figure 8.** Chart of modes of microjet flow and breakup into microdrops with indicated boundaries of transitions between them, represented via liquid flowrates and concentrations of polymer in the solution (a) and via dimensionless similarity criteria Oh and Re (b);  $f = 1000$  Hz.

microdrops. Fig. 8 also shows another differences in the determination of boundaries between the modes of breakup into microdrops. The identified shifts of liquid flowrate ranges for the compounds under study are determined by adjustment of the balance between parameters of the external excitation and the nature of the liquid that interacts with this impact. Also, the formation of „beads-on-string“ type structures for the 5 mg/ml ALG solutions at liquid flowrates of 7–26 ml/min (Fig. 3) should be included in the set of features of the unstable behavior related to the nature of liquid with viscoelastic properties. With a growth of liquid flowrate the liquid bridges become larger in diameter and length, which promotes polydispersity of microdrops in the flow. However, at a liquid flowrate of 7–9 ml/min

the coalescence of satellite microdrops is relatively quick, therefore the mode is conventionally named monodisperse, by groups of 2–4 main microdrops.

In the case of simultaneous analysis of microjet flow and breakup to microdrops modes, it is important to note that the intensity of vibration excitation, which is dependent on a number of above-mentioned factors, excites a laminar flow providing for the diversity of amplitudes and wavelengths within the microjet. The mode of monodisperse breakup into microdrops can be established at these set characteristics. In the literature, for the purpose of universalization of the unstable flow behavior dimensionless and dimension parameters are often used [7,28]: wave number  $k$  ( $k = \pi D \lambda_w^{-1}$  where  $D$  — microjet diameter, [m],  $\lambda_w$  — wavelength of

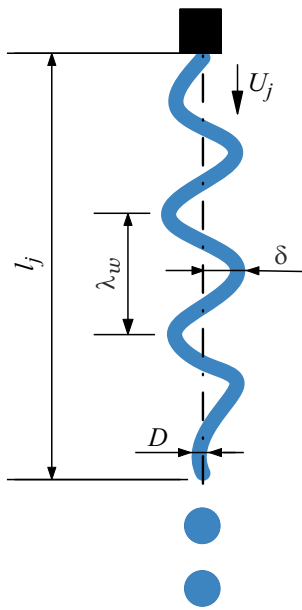


**Figure 9.** Microjet laminar flow diagram with physical parameters shown.

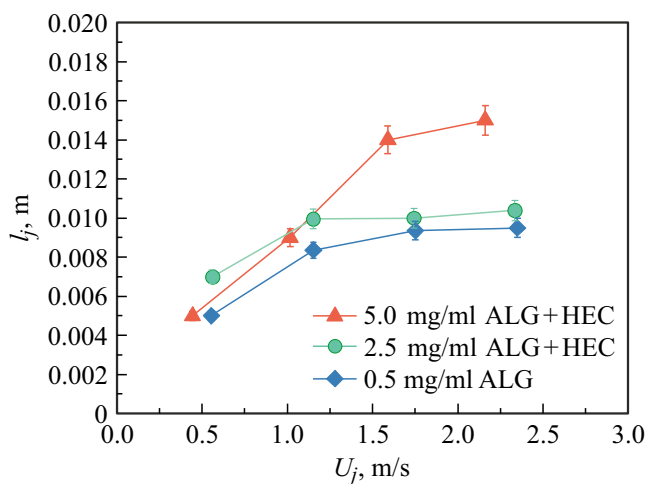


**Figure 10.** Dependence of microjet breakup length  $l_j$  on microjet velocity  $U_j$  for three liquids under study at liquid flowrates of 5, 10, 15, and 20 ml/min (correspond to point positions within the curves, from left to right) and  $f = 1000$  Hz.

microjet perturbation, [m] (Fig. 9)), dimensionless perturbation amplitude  $\delta/D$  or  $2\delta/D$ , where  $\delta$  — initial amplitude of the microjet perturbed by an external impact, [m] (Fig. 9), as well as length of microjet breakup  $l_j$ , [m].

In particular, an attempt is made to identify the dependence of microjet breakup length  $l_j$  (schematically shown in Fig. 9) on its velocity  $U_j$ . Fig. 10 shows that growth of velocity  $U_j$  in all cases resulted in an increase in values of  $l_j$  at  $f = 1000$  Hz. At the same time an increase in polymer concentration in the solution up to 5 mg/ml allowed achievement of a significant increase (up to 50%) in values of  $l_j$  at increased flowrates (15 and 20 ml/min), which most

likely is connected to the more noticeable manifestation of the contribution of increased viscosity and surface tension coefficient for the most concentrated polymer solution (see the table) at increased values of  $U_j$ .

### 3.3. Influence of the external perturbation current frequency on the capillary breakup of microjet

To find out the role of the external vibration perturbation current frequency in the formation of behavior patterns (systems of arrangement in the flow) of main and satellite microdrops, the capillary breakup of all solutions under test was investigated at a liquid flowrate of 6 ml/min and  $f$  values of 0, 400, 800, 1200 Hz. Fig. 11 shows results of such investigation for the 0.5 mg/ml ALG + HEC solution.

First of all, with activation of the piezoactuator a clear increase in the microjet breakup length  $l_j$  by 7% is noted in comparison with the case of its natural instability without external impact. However, at the same time average values of  $l_j$  decrease with the growth of  $f$  (at  $f = 800$  Hz  $l_j$  is decreased by 3–4% in comparison with  $f = 400$  Hz, while at  $f = 1200$  Hz  $l_j$  is decreased by another 17%), as well as the diameter  $d$  of microdrops separating from the microjet (Fig. 11). At  $f = 400$  Hz the microjet starts breaking up in the „by groups“ mode with long intervals out of the groups of microdrops (Fig. 11, *b*). When  $f = 800$  Hz, the phenomenon of drop grouping is not so noticeable, because distances between drops tend to the equidistant case (Fig. 11, *c*). These conditions can be denoted as transient, because at  $f = 1200$  Hz a steady monodisperse microjet breakup is achieved. The formed microdrops

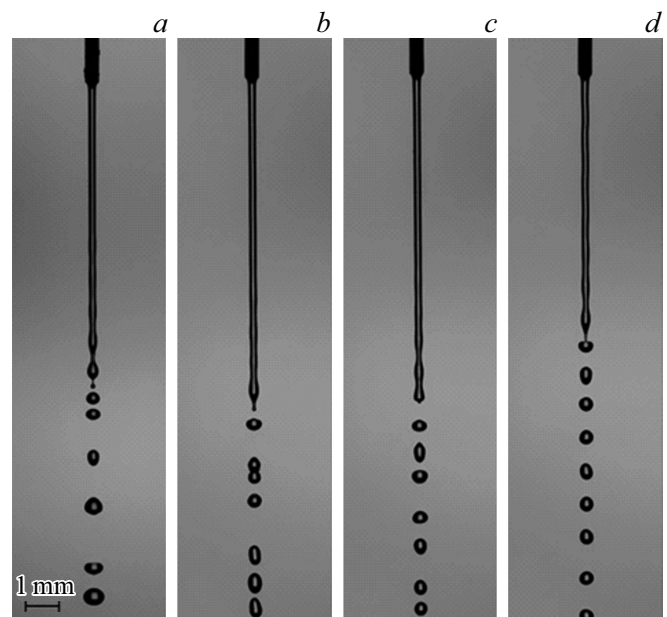


**Figure 11.** Visualization of the process of microjet breakup for the 0.5 mg/ml ALG + HEC polymer solution at a liquid flowrate of 6 ml/min and the following frequencies of the external vibration excitation current,  $f$ : 0 (*a*), 400 (*b*), 800 (*c*),  $f = 1200$  Hz (*d*).

have a homogeneous shape (close to the spherical shape) and nearly identical sizes, and they are also equidistant to each other in the flow with insignificant and rare deviations, at least within a distance of  $15d-20d$  in relation to the microjet breakup region (Fig. 11, *d*). At  $f \geq 800$  Hz changes in  $l_j$  and  $d$  become less noticeable and forecastable with increase in polymer concentration in the solution. The latter fact is related to the formation of liquid bridges, which, as it was mentioned above, slow down and disarrange the capillary breakup of the microjet.

Varying the values of  $f$  with keeping constant other system parameters is an effective and giving the most good forecasts tool to adjust behavior patterns of microdrops after the capillary microjet breakup, their homogeneity in terms of shape (spherical) and physical size, as well as to determine values of  $l_j$ . The reliability of forecasting is due to the fact that the liquids under study, i.e. diluted polymer solutions, have demonstrated involvement in the above-described patterns at the same values of  $f$  with the trends kept as related to the geometric shape and physical size, as well as values of  $l_j$ .

## Conclusion

The cause of formation of the system of grouped arrangement of microdrops in a flow after the capillary microjet breakup is determined. It is shown that „beads-on-string“ type structures for the 5 mg/ml ALG destabilize the process of microjet breakup. Cases are recorded when no satellite microdrops are formed from the liquid filaments between main microdrops. Three modes of microjet flowing and three modes of breakup of laminar microjet flow into microdrops are distinguished. The influence of viscosity and surface tension coefficient of the liquid on the change in the microjet breakup length at increased liquid flowrates (15 and 20 ml/min) is shown. Conditions of the controlled monodisperse breakup into microdrops are determined, where the microjet profile before the capillary breakup can be both linear and wavy. The significance of adjustment of the optimum balance between the molecular mass of polymer in the solution, the intensity of external perturbation, and the stress relaxation time in polymer viscoelastic materials to achieve the monodisperse microjet breakup with equidistant arrangement of main microdrops in the flow is demonstrated. It is found that the adjustment of external vibration perturbation current frequency with keeping constant other system parameters is the most reliable tool to forecast behavior patterns of microdrops after the capillary microjet breakup, their homogeneity in terms of spherical shape and physical size, as well as values of the microjet breakup length.

## Funding

This study was supported by grant № 22-29-20109 from the Russian Science Foundation (<https://rscf.ru/project/22-29-20109/>) and the Administration of the Tomsk Region.

## Conflict of interest

The authors declare that they have no conflict of interest.

## References

- [1] H. Wijshoff. *Phys. Rep.*, **491**, 77–177 (2010). DOI: 10.1016/j.physrep.2010.03.003
- [2] D. Serp, E. Cantana, C. Heinzen, U. Von Stockar, I.W. Marison. *Biotechnol. Bioeng.*, **70**, 41–53 (2000). DOI: doi.org/10.1002/1097-0290(20001005)
- [3] C.W. Visser, T. Kamperman, P.L. Karbaat, D. Lohse, M. Karperien. *Sci. Adv. American Association for the Advancement of Science*, **4** (2018). DOI: 10.1126/sciadv.aao1175
- [4] M. Neukötter, S. Jesinghausen, H.-J. Schmid. *Rheol. Acta*, **61**, 499–521 (2022). DOI: 10.1007/s00397-022-01339-y
- [5] F. Del Giudice, S.J. Haward, A.Q. Shen. *J. Rheol. (N.Y.N.Y.)*, **61**, 327–337 (2017). DOI: 10.1122/1.4975933
- [6] D. Baumgartner, G. Brenn, C. Planchette. *Phys. Rev. Fluids*, **5**, 103602 (2020). DOI: 10.1103/PhysRevFluids.5.103602
- [7] Y. Christanti, L.M. Walker. *J. Rheol. (N.Y.N.Y.)*, **46**, 733–748 (2002). DOI: 10.1122/1.1463418
- [8] N. Blanken, M.S. Saleem, M.-J. Thoraval, C. Antonini. *Curr. Opin. Colloid Interface Sci.*, **51**, 101389 (2021). DOI: 10.1016/j.cocis.2020.09.002
- [9] A.E. Ashikhmin, N.A. Khomutov, M.V. Piskunov, V.A. Yanovsky. *Appl. Sci.*, **10** (2020). DOI: 10.3390/app10020685
- [10] M. Piskunov, A. Semyonova, N. Khomutov, A. Ashikhmin, V. Yanovsky. *Phys. Fluids*, **33**, 83309 (2021).
- [11] M. Piskunov, A. Semyonova, N. Khomutov, A. Ashikhmin, V. Yanovsky. *Int. J. Heat Mass Transf.*, **185**, 122442 (2022). DOI: 10.1063/5.0059079
- [12] J. Eggers. *Rev. Mod. Phys.*, **69**, 865–930 (1997). DOI: 10.1103/RevModPhys.69.865
- [13] A.H. Lefebvre, V.G. McDonell. *Atomization and Sprays*, **2**, 300 (2017). DOI: 10.1201/9781315120911
- [14] W.T. Pimbley, H.C. Lee. *IBM J. Res. Dev.*, **21**, 21–30 (1977). DOI: 10.1147/rd.211.0021
- [15] J.H. Hilbing, S.D. Heister. *Phys. Fluids*, **8**, 1574–1581 (1996). DOI: 10.1063/1.868931
- [16] A.U. Chen, O.A. Basaran. *Phys. Fluids*, **14**, L1–L4 (2002). DOI: 10.1063/1.1427441
- [17] U. Prüße, J. Dalluhn, J. Breford, K.-D. Vorlop. *Chem. Eng. Technol.*, **23**, 1105–1110 (2000). DOI: 10.1002/1521-4125(200012)23:12
- [18] T. Kamperman, V. Trikalitis, M. Karperien, C.-W. Visser, J. Leijten. *ACS Appl. Mater. Interfac.*, **10**, 23433–23438 (2018). DOI: 10.1021/acsami.8b05227
- [19] V. Nedović, V. Manojlović, U. Pruesse, B. Bugarski, J. Djonlagić, K. Vorlop. *Chem. Ind. Chem. Eng. Q.*, **12**, 53–57 (2006). DOI: 10.2298/CICEQ0601053N
- [20] D. Baumgartner, W. Bernard, B. Weigand, G. Lamanna, G. Brenn, C. Planchette. *J. Fluid Mech.*, **885** (2020). DOI: 10.1017/jfm.2019.967
- [21] D. Baumgartner, G. Brenn, C. Planchette. *Int. J. Multiph. Flow.*, **150**, 104012 (2022). DOI: 10.1016/j.ijmultiphaseflow.2022.104012
- [22] D. Baumgartner, G. Brenn, C. Planchette. *J. Fluid Mech.*, **937** (2022). DOI: 10.1017/jfm.2022.107

- [23] C. Liu, T. Jin, W. Liu, W. Hao, L. Yang, L. Zheng. *LWT*, **148**, 111770 (2021). DOI: 10.1016/j.lwt.2021.111770
- [24] D.W. Bousfield, R. Keunings, G. Marrucci, M.M. Denn. *J. Nonnewton. Fluid Mech.*, **21**, 79–97 (1986). DOI: 10.1016/0377-0257(86)80064-7
- [25] J. Li, M.A. Fontelos. *Phys. Fluids*, **15**, 922–937 (2003). DOI: 10.1063/1.1556291
- [26] C. Clasen, J. Eggers, M. Fontelos, J. Li, G. McKinley. *J. Fluid Mech.*, **556**, 283–308 (2006). DOI: 10.1017/S0022112006009633
- [27] R. Sattler, S. Gier, J. Eggers, C. Wagner. *Phys. Fluids*, **24**, 23101 (2012). DOI: 10.1063/1.3684750
- [28] R.P. Mun, J.A. Byars, D.V. Boger. *J. Nonnewton. Fluid Mech.*, **74**, 285–297 (1998). DOI: 10.1016/S0377-0257(97)00074-8